J Mater Sci (2014) 49:786–793
DOI 10.1007/s10853-013-7761-3

Low-temperature processing of thin films based on rutile TiO_2 nanoparticles for UV photocatalysis and bacteria inactivation

Joel Molina · Jose Luis Sanchez-Salas · Carlos Zuniga · Eunice Mendoza · Rosalia Cuahtecontzi · Gabriela Garcia-Perez · Edmundo Gutierrez · Erick R. Bandala

Received: 9 July 2013 / Accepted: 20 September 2013 / Published online: 28 September 2013

Abstract Using a low-temperature, simple, and economic processing technique, TiO_2 nanoparticles (rutile phase) are immobilized in an inorganic matrix and then deposited on glass for bacteria inactivation in water. Using this low thermal budget method (maximum processing temperature of 220 °C), thin films of immobilized TiO_2 nanoparticles are obtained so that practical water decontamination after UV radiation is possible by avoiding the additional step of catalyst separation from treated water. In order to validate the photocatalytic activities of these TiO_2 nanoparticles (prepared as thin films), they were tested for bacteria inactivation in water under UV–A radiation ($\lambda > 365$ nm), while extensive characterizations by dynamic light scattering, X-ray diffraction, ultra violet–visible absorption spectroscopy, fourier-transform infra red spectroscopy, and profilometry were also carried out. Despite previous reports on the low or lack of photocatalytic activity of rutile-phase TiO_2, inactivation of *Escherichia coli* in water was observed when thin films of this material were used when compared with the application of UV radiation alone. Physical characterization of the films suggests that size and concentration-related effects may allow the existence of photocatalytic activity for rutile-TiO_2 as long as they are exposed under UV–A radiation, whereas no effect on bacteria inactivation was observed for thin films in the absence of TiO_2 or radiation. In brief, a low thermal budget process applied to thin films based on TiO_2 nanoparticles has shown to be useful for bacteria inactivation, while possible application of these films on widely available substrates like polyethylene terephthalate materials is expected.

J. Molina (✉) · C. Zuniga · E. Gutierrez
Electronics Department, National Institute of Astrophysics, Optics and Electronics (INAOE), Luis Enrique Erro #1, 72840 Sta. Maria Tonantzintla, Puebla, Mexico
e-mail: jmolina@inaoep.mx

J. L. Sanchez-Salas · E. Mendoza · R. Cuahtecontzi · G. Garcia-Perez · E. R. Bandala
Grupo de Investigacion En Energia y Ambiente, Universidad de las Americas, Puebla (UDLAP), Sta. Catarina Martir, 82710 Cholula, Puebla, Mexico

Introduction

In recent years, introduction of nanostructured materials for water-treatment applications has resulted in highly efficient solutions for water decontamination given their large contact surface areas, and therefore, higher photocatalytic activity presented by many of the nanoparticles, nanotubes, nanorods, nanomembranes, and other available nanostructures [1–3]. In particular, bacteria inactivation using TiO_2 nanoparticles (whether doped or undoped) has shown promising results because they produce fast and complete degradation of organic pollutants given their highly reactive properties (enhanced light absorption due to the large fraction of surface atoms) compared with highly dense TiO_2 thin films [4, 5]. However, the separation of particle-type photocatalysts from the solution following the photocatalytic process can be very difficult, and the tendency of the particles to agglomerate into larger particles effectively reduces the photocatalytic activity during cyclic use. Therefore, it is important to consider nanoparticle-based materials like TiO_2, which can be later embedded in a suitable host matrix and then used as thin films to promote an enhanced photocatalytic activity (compared with dense bulk films having smaller contact surface area), and without the additional step of catalyst separation.

From the point of view of photocatalytic applications, there are two main crystal phases commonly associated with

TiO_2: rutile and anatase. The first one usually identified as possessing no photocatalytic activity at all or slightly contributing only when anatase phase is present in the oxide's crystal lattice [6]. Some reports have suggested that pure rutile has some photocatalytic activity depending on the preparation procedure, the nature of the precursors or the nature of the organic compound used as reducing reagent. The role of rutile in photocatalytic processes seems to be important only when the photocatalyst is prepared including a mixture of both phases, but these studies are more related to the mathematical approach used for comparison among the experimental results rather than to the physical or chemical contribution of the rutile phase [6]. Rutile-phase TiO_2 synthesis has, however, attracted great interest due to its optical and electrical properties as well as an interesting academic challenge since synthesis of rutile nanocrystals is much more difficult than anatase [7]. Photocatalytic activation of rutile-phase TiO_2 has been attempted at different extents by its synthesis as nanorods [7], or by doping with metals like Ag [8], Ni [9], or nonmetals such as I [10], N [11], C, and S [12, 13]. However, the effect of iodine doping on the photoactivity of rutile remains under debate, and the improvement of its photoactivity using N, C, or S as dopant has been reported as relatively poor.

In this study, we present our experimental results on the preparation, structural characterization, and photocatalytic activity of rutile-phase undoped TiO_2 nanoparticles either as free suspension or immobilized as thin films (using an inorganic based matrix) and their application in the inactivation of bacteria (*E. coli*) in water. During preparation of the resulting films, a low thermal budget process ($T \leq 220$ °C) was used to promote the application of this material on readily available PET or any other flexible substrate (after chemical modification of their surfaces for enhanced adhesion of the films) for widespread use.

Materials and methods

Synthesis of thin films based on rutile-phase TiO_2 nanoparticles

Low-organic content or silicate-type spin-on glass (SOG)-based SiO_2 (700B from Filmtronics, Corp.) was used as matrix for immobilization of TiO_2 nanoparticles. The average diameter of TiO_2 nanoparticles used was 360 nm before synthesis (R-706 with 93 % purity, as stated by Dupont). Initially, specific amount of commercial TiO_2 was suspended in deionized water by hydrolyzing this TiO_2:H_2O mixture in a water bath (45 °C, with variation of ±2 °C, 30 min) and then SOG-based SiO_2 was added. The final TiO_2:SiO_2:H_2O mixture was again heated in a water bath (80 °C, 1 h) to obtain a stable TiO_2 suspension

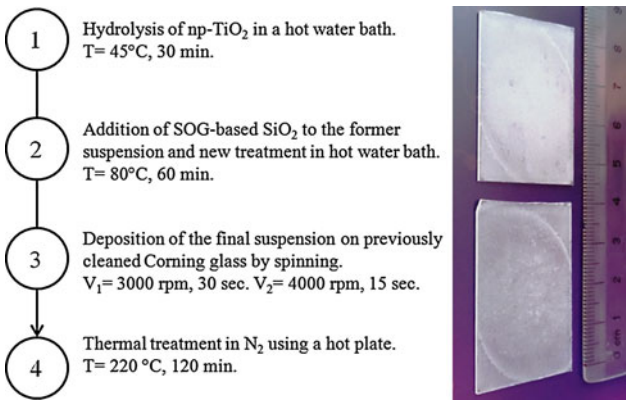

Fig. 1 Process flow for the preparation of thin films based on rutile-phase TiO_2 nanoparticles and deposited on glass at very low temperatures. Two actual samples obtained by this method are shown, and we notice a good uniformity of the resulting films after deposition on these large area substrates

(minimizing nanoparticles' aggregation and/or sedimentation). The concentration ratios of TiO_2 to SiO_2:H_2O were 200, 100, 50, and 10 mg mL^{-1} and these suspensions were labeled as A, B, C, and D, respectively. Each concentration of TiO_2 nanoparticles was measured with an analytic balance AG285 from Mettler-Toledo. The final TiO_2:SiO_2:H_2O suspensions were directly applied on one surface of clean glass slides (2947, size of 75 mm × 25 mm, from Corning) and sequentially spun first at 3000 rpm, 30 s, and then 4000 rpm, 15 s to obtain uniform thin layers of TiO_2 embedded in SiO_2. These were the best spinning conditions to obtain films with good characteristics and avoid thickness nonuniformities, pinholes, striations, and/or excessive film being deposited at the back of the glass slides. After spinning, all films (A–D) were baked for 2 h using a hot plate at 220 °C under N_2 flow (99.99 % purity) to evaporate mostly water and some of the organic solvents present in the SOG-based SiO_2 matrix [14]. For FTIR characterization, the same processing sequence was followed, and the final suspension was applied on prime-grade P-type silicon wafers (100) with resistivity of 5–10 Ω cm to eliminate most of the organic and impurity elements present within the Corning glass slides. Given the ultra-low thermal budget required for fabrication of these simple structures, their introduction into flexible substrates with large area is expected, thus promoting widespread use of optimized films. The process flow for fabrication of the structures is briefly summarized in Fig. 1 along with a picture of two Corning glasses covered with the resulting films (suspensions A and B only).

Chemical and physical characterizations

DLS measurements (Nanotrac Wave, from Microtrac) were done to determine the final size distribution of TiO_2

nanoparticles after the whole synthesis process. Also, thicknesses for all films were measured by profilometry (DEKTAK, V200-SI) after partially etching the TiO_2/SiO_2 film using a strong acid solution composed of diluted HF (HF:H_2O, 1:2 volume ratio). The crystalline phases of the resulting TiO_2-based films were obtained after X-ray diffraction (XRD) measurements (Empyrean, from PANalytical), with a scanning step of 0.02°, using Cu-Kα radiation with $\lambda = 1.5406$ Å as an X-ray source. The band-gap energies E_g of the resulting films were calculated using optical transmittance data measured using an UV–Vis absorption spectrometer (LAMBDA 3B with double beam from Perkin Elmer, Inc., and using Corning glass as substrate) and the Tauc method [15, 16]. Chemical compositional analyses for all films were obtained by FTIR spectrum measurements in absorbance mode using a Bruker Vector-22 system after 5 min of purge in N_2. The samples were measured against crystalline silicon substrate or SOG-based silicon dioxide on glass (both used as references).

E. coli inactivation assessments

The bacterial strain used in the experiments was *E. coli* ATCC 25922 (American Type Culture Collection). Microorganisms were acquired from the UDLAP microbial collection. The bacteria were kept frozen at −80 °C on Tryptic Soy Broth (TSB) and 20 % glycerol. Before each experiment, the phenotype of the culture was validated streaking on McConkey agar for colony morphology and biochemical features using the 32 GN miniAPI® galleries, and the semiautomatic miniAPI® reader. *E. coli* was grown on TSB and Tryptic Soy Agar (TSA), in liquid and solid culture media, respectively. Cells were acquired from an overnight plate culture incubated at 37 °C under aerobic conditions. Cells were inoculated to 10 mL TSB and incubated at the same conditions on a water bath rotary shaker at 200 rpm. Bacterial growth was monitored by means of optical density at 600 nm, and cells at exponential growth phase were collected and used immediately at the required cell density, adjusting with McFarland standard, to obtain an initial concentration of c.a. 10^5 CFU mL^{-1}.

System for bacterial inactivation

The suspension of TiO_2 (rutile or anatase phase, r-TiO_2 or a-TiO_2) or glass slides with r-TiO_2 thin films (immobilized within SOG at different concentrations) were added to 20 mL of water in a Petri dish and a magnetic bar. The system was then sterilized by an UV disinfection lamp (260 nm radiation) in a sterile guard hood type II by 20 min. The sterile condition was confirmed by seeding the sample into a TSB or TSA, and the absence of bacterial growth was observed. Then the bacteria were added to the Petri dish to have an initial bacteria concentration of $\sim 10^5$ CFU mL^{-1}. The Petri dishes were placed on a magnetic stirrer and irradiated with UV ($\lambda_{max} = 334$ nm) at a distance of 7 cm. The radiation flux obtained at the surface of the Petri dishes was 9.7 μW cm^{-2} (measured by a radiometer). Samples of 0.1 mL were collected at different periods of time (0, 15, 30, 45, 60, 75, 90, 105, and 120 min). Every sample was diluted by multiples of ten (from 10^{-1} to 10^{-8}), and 10 μL of each dilution was dropped in TSA, divided into squares of 1.5 cm^2. Colony-forming units (CFUs) were counted for every dilution to obtain the amount of bacteria survivors per milliliter.

Results and discussion

DLS and profilometry results

As result of synthesis of the corresponding suspensions, Fig. 2 shows the average TiO_2 particle diameters for two conditions: as-prepared (measured after at least 24 h of settling time of the synthesized suspensions) and right after sonication using an ultrasonic vibrator (Branson B1510, 2 min at 40 kHz and room temperature). The dotted arrow shows the nominal average diameter as stated by the manufacturer and which is located at about 360 nm. The as-prepared samples present a larger particle diameter because of their tendency to agglomerate or aggregate after dispersion and settling within a liquid suspension. During sonication, enhanced dispersion of TiO_2 agglomerates is obtained by overcoming their weaker attractive forces, the final result being smaller TiO_2 nanoparticle diameters. The average physical size for sonicated r-TiO_2 nanoparticles is around 300 nm. Figure 2 also shows the final TiO_2 film's thickness after deposition (by spinning on silicon) and thermal treatment of the prepared suspensions. Thicker TiO_2 films were obtained for more concentrated suspensions as expected. As reference, film thickness of SOG-based oxide alone (without dilution in H_2O) was about 400 nm, which compares well with data obtained for similar spinning conditions [14]. Since all A–D suspensions were prepared using different TiO_2:SiO_2:H_2O volume ratios (see the experimental procedure), different concentrations of TiO_2 within the same matrix would produce different thin film thicknesses. A similar trend of thickness reduction for SiO_2 when diluted using different percentages of H_2O was also found by Molina et al. [14] and final thickness of SiO_2 could be further reduced when the samples were annealed at higher temperatures. Given that for sample D there is a minimum amount of TiO_2 nanoparticles (only 10 mg mL^{-1}), the final average thickness

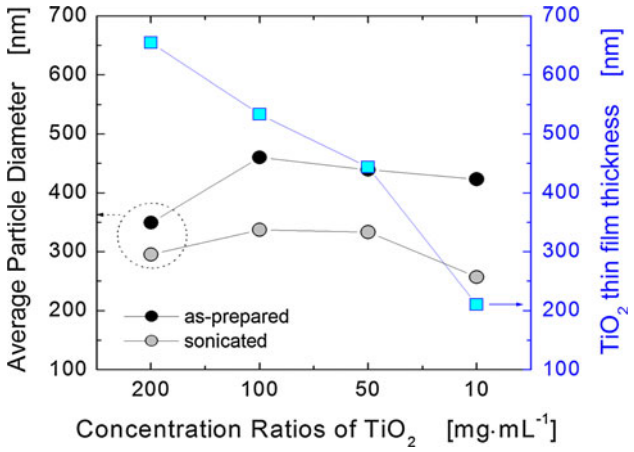

Fig. 2 DLS and profilometry data showing the average TiO_2 particle diameter and the resulting thin film thickness, respectively (after depositing this material on glass surfaces)

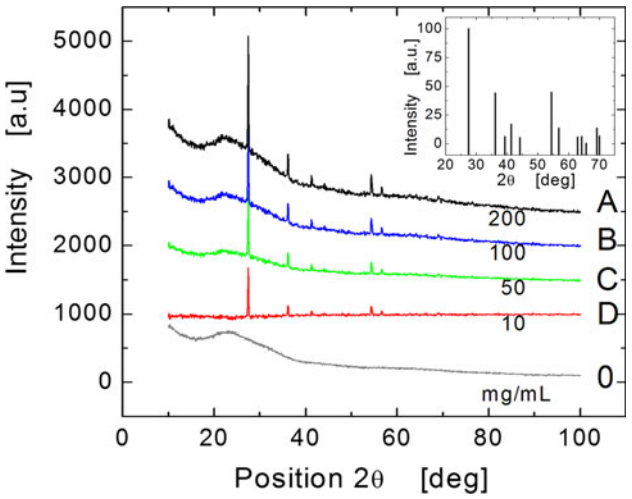

Fig. 3 XRD data for TiO_2 films fabricated in this study. Sample 0 (SiO_2/glass structure) is also shown as reference

for this film was kept below the average nanoparticles' diameter because of the reduction in most of the SiO_2 thickness by enhanced H_2O dilution and also, because larger amount of water per volume induces further dilution or dispersion of previously agglomerated TiO_2 nanoparticles. Finally, it is important to notice that since these films will be in direct contact with contaminated water, measurements of the nanoparticles' sizes and their distribution at both the film's surface and in the bulk are necessary to mainly correlate surface distribution of nanoparticles to photocatalytic activity. These measurements could be done by scanning electron microscopy (SEM) or atomic force microscopy (AFM) for the surface, while transmission electron microscopy (TEM) could be done to obtain the characteristics of the nanoparticles in the bulk of the embedding matrix. These last measurements are actually under progress, and the results will be published elsewhere.

XRD results

After obtaining TiO_2-based thin films, Fig. 3 shows the XRD diffraction patterns for all thin films including sample 0 (SOG), which is only the amorphous matrix of SiO_2 deposited atop the glass slides and cured at the same temperature. It is clear that sample 0 does not present the characteristic sharp diffraction peaks of a crystalline material because the incident X-rays are scattered in many directions leading to a large bump distributed over a wide range of 2θ, just like the one shown here for reference purposes. Samples C–D present the lowest intensities for the diffraction peaks related to the crystalline phase of TiO_2, since their nanoparticle concentrations were quite small, (50 and 10 mg mL^{-1}, respectively). On the other hand, samples A–B (with concentrations of 200 and 100 mg mL^{-1}, respectively) clearly present the characteristic sharp diffraction peaks for rutile-phase TiO_2 including the broad amorphous phase from both the SiO_2 matrix and the glass slide (used for TiO_2 immobilization and mechanical support purposes, respectively). In particular, sample A showed the clearest and highly intense diffraction peaks which fit well with those of standard rutile TiO_2 (Powder Diffraction File No. 21-1276). The inset in Fig. 3 shows the main diffraction peaks calculated directly by the XRD equipment right after the measurement of sample A. These results provide the evidence of the existence of rutile phase in the thin TiO_2 films after using high TiO_2 nanoparticle concentrations (at least 50 mg mL^{-1}).

IR spectrum (in absorbance mode) of TiO_2

The IR spectra for all samples are shown as absorption coefficient α after normalization of each sample to a single and averaged TiO_2 film thickness. Since these samples are quite different for bulk and dense TiO_2 thin films, the TiO_2 nanoparticles tend to disperse within the SiO_2 matrix (generating empty spaces) thus avoiding normalization with respect to each physical thickness. The initial IR measurements were done at wavenumber between 1600 and 400 cm^{-1}, and they were adjusted using the SOG-based oxide film as reference (SiO_2/Glass), in order to eliminate the influence of the highly absorbent peaks related to Si–O and Si–O–Si bonds [17, 18]; especially those found at 1070 and 443 cm^{-1}, and which could screen-out the presence of any detectable Ti–O–Ti bonds; see Fig. 4. The obtained IR spectra include some absorption bands at 765 (black arrow at shoulder section), 530, and 395 cm^{-1}. The band detected as a shoulder at 765 cm^{-1} is comparable with the IR spectrum of

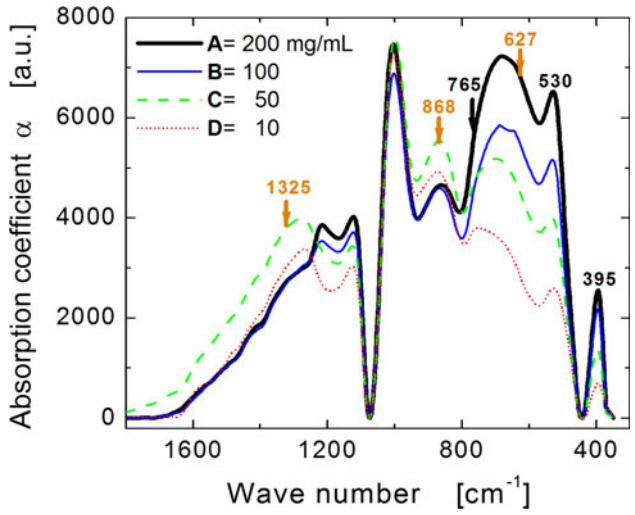

Fig. 4 IR spectra in absorbance mode of TiO_2 for all A–D samples, and obtained using SiO_2/glass as reference

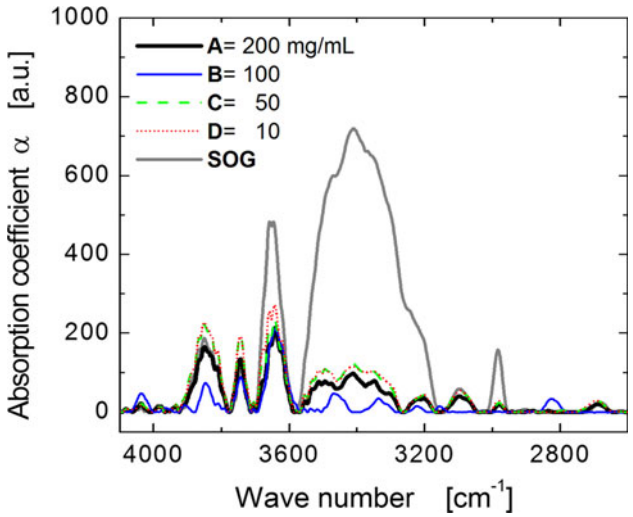

Fig. 5 IR spectra in absorbance mode of TiO_2/SiO_2 samples for wavenumbers ranging from 4000–2600 cm^{-1} region

crystalline TiO_2 (having anatase or rutile crystalline structure) due to symmetric stretching vibrations of the Ti–O bonds [19]. The absorption peaks for these Ti–O bonds increase with the content of TiO_2, confirming proper chemical bonding of this photocatalytic material for even the larger TiO_2 concentrations. Also, even though the main absorption bands for the Si–O–Si bonds mostly disappear when SOG-based oxide film is used as reference, some Si–O bonds appear in these samples surely because of vibrations of Si–O–Ti bonds, as observed in the band at 1005 cm^{-1}. On the other hand, the bands at 627 and 1325 cm^{-1} are thought to be related to vibrations of some Al–O bonds, while the band at 868 cm^{-1} is related to a combination of both Al–O and Si–O bonding vibrations [20]. All these contributions make sense considering that commercial TiO_2 nanoparticles consist, according to the manufacturer, of 93 % TiO_2, 2.5 % Al_2O_3 and 3 % SiO_2 (the remaining percentage consisting of other undetectable elements).

Figure 5 shows the absorption spectra of TiO_2/SiO_2 films from 4000 to 2600 cm^{-1}, where the presence of strong absorption bands in the region of 3200–3500 cm^{-1} is noticed (corresponding to bending vibrations of adsorbed and possibly coordinately bounded OH molecules with Ti or Si). Also, the weak absorption peaks in the region of 2920–2930 cm^{-1} among others are related to the presence of organic residues that were not fully evaporated or decomposed during the low-temperature thermal treatments applied to the TiO_2 films [21]. For comparison, the IR spectra for SOG-based oxide are also shown so that the main absorption bands related to purely organic elements can be easily identified (having the strongest absorption peaks). Since the highest thermal treatment applied to all A–D samples was only 220 °C, higher temperatures for this final curing process would evaporate or reduce these organic residuals more efficiently. However, for practical applications, it is desired to reduce the total thermal budget for this material so that it could be possible to develop coatings of TiO_2 (with enough photocatalytic activity) on plastic or other economic and readily available flexible substrates for large area applications.

On the other hand, measuring the precise chemical composition of the films' surface could be done using Angle-Resolved X-ray Photoelectron Spectroscopy (AR-XPS), a high-energy spectroscopic technique that is able to give both the chemical and electronic states of the first 10 nm of the film's thickness. However, great care must be taken into account to reduce evaporation of the embedding matrix within the measurement chamber because of the ultra-high vacuum conditions needed for these measurements. These data, along with electron microscopy measurements will be carried out for films based on np-TiO_2 having higher thermal treatments (using quartz as substrate), and the results will be published elsewhere.

UV–Vis spectra analysis of TiO_2

Optical band gap is an important parameter in semiconductor materials because it allows knowing the threshold energies to which a material in particular, like TiO_2, is "transparent" or able to absorb incident photons. and therefore, create electron–hole pairs that could participate in photocatalytic processes. The UV–Vis spectra from 190 to 900 nm region for the different TiO_2 concentrations (A–D samples), including the spectrum for only the glass substrate, are all shown in Fig. 6. It can be seen that strong absorption occurs at wavelengths $\lambda < 290$ nm (UV-B spectrum) for all samples and that transmittance is reduced

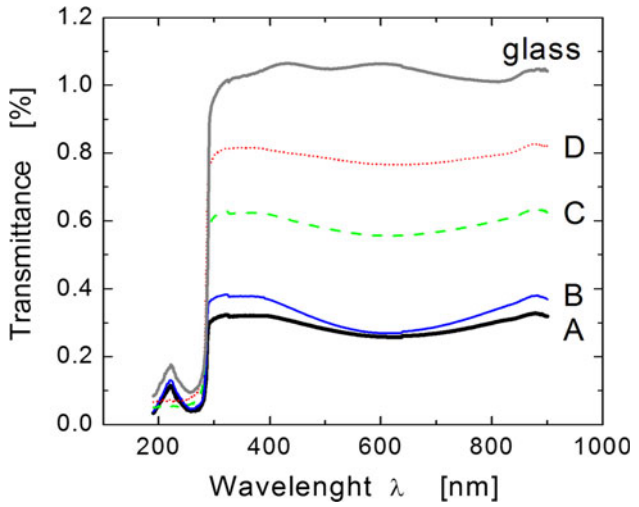

Fig. 6 UV–Vis spectra obtained for all TiO_2/SiO_2 (*A–D*, *glass*) samples showing that transmittance is inversely proportional to TiO_2 concentration

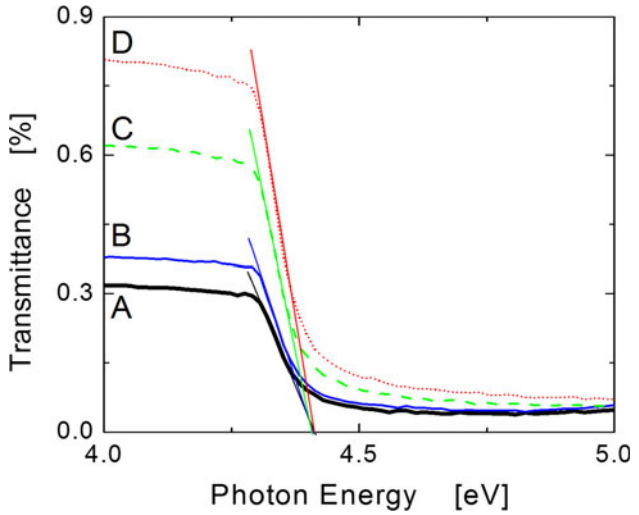

Fig. 7 Extrapolation of UV–Vis transmittance data to photon energy for all *A–D* samples in order to obtain TiO_2 band-gap energy (E_g)

in direct proportion to the TiO_2 concentration as expected. Even though the physical thicknesses for all samples are different (see Fig. 2), only slight variations in their optical band gaps are expected if we consider similar densities for these films. In addition, since the number of interference fringes is not visible, this avoids using the Swanepoel model for optical band-gap calculation E_g [22], and therefore, a fast estimation was done to obtain this important parameter. Figure 7 shows the transmittance spectra versus photon energy for the A–D samples. The inflexion point is the crossing for all samples after linearly extrapolating all slopes with the axe for photon energy. The band gap E_g is determined by dividing this inflexion point by $\sqrt{2}$, [23]. The inflexion points cut the photon energy axis at between 4.41 and 4.42 eV so that the correspondent

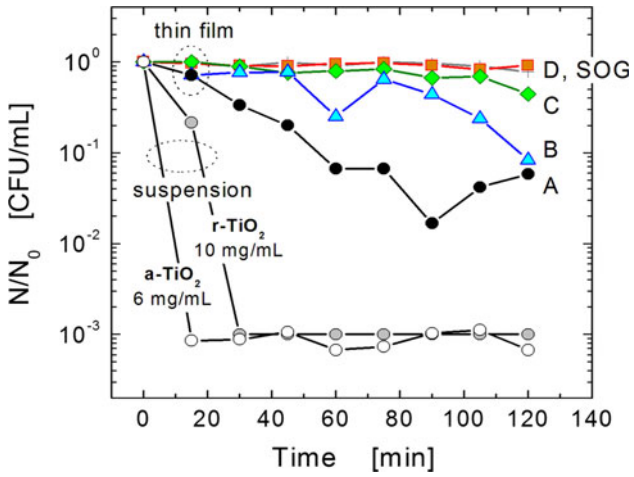

Fig. 8 Survival rates of *E. coli* (after normalization to its original concentration) after introduction of TiO_2 nanoparticles in both suspension (showing anatase and rutile phases for TiO_2) and thin film structures (*A–D* samples). No photocatalytic activity is shown for *D* and SOG samples

optical band gap E_g values for all A–D samples occur at 3.11–3.12 eV. This band-gap energy E_g corresponds with the reported E_g for anatase or rutile TiO_2, between 3.0 and 3.2 eV, respectively [24, 25].

Antibacterial activity results

Figure 8 shows that the TiO_2 anatase phase is highly active with UV light (364 nm) at 6.0 mg mL^{-1} in suspension form (these anatase phase TiO_2 nanoparticles were synthesized at UDLAP). TiO_2 in rutile phase is also moderately active for bacteria inactivation in suspension but requiring a concentration of 10 mg mL^{-1} and almost the double of time. For thin films composed of rutile TiO_2 having the highest nanoparticle concentration (sample A), the bacteria elimination activity is rather moderate and slow, since the required time for maximum bacteria inactivation is in the range of around 60–90 min as compared with its suspension form. Thin films of rutile TiO_2 with lesser nanoparticle concentration (samples B–D) produce minimum disinfection activity as shown in Fig. 8. A thin film of spin-on glass alone (SOG sample) or distillated water has no disinfection activity at all for the same experimental conditions, meaning that all disinfection activities are due to rutile-phase TiO_2. It is important to notice that even though the initial concentration of rutile TiO_2 was 200 mg mL^{-1} in suspension form (A sample), fabrication of thin films using this material requires depositing this suspension on glass plates (whose area is 18.5 cm^2), spinning those plates at high velocities and, because of centrifugal forces, the remaining amount of solid TiO_2 is less compared with its original content in suspension form. For up to four sequential deposition runs of

np-TiO_2 on the same glass slide (sample A, similar conditions), we measured the change in weight of the glass slide before and after deposition/annealing, and the remaining content of np-TiO_2:SiO_2:H_2O is roughly 65 % of the original value (considering a density of 200 mg mL^{-1} in suspension form for sample A). On the other hand, measuring the accurate concentration of np-TiO_2 only at the surface of the deposited film is quite difficult, and it would require dedicated surface analysis for large areas.

In addition, a lower disinfection activity for thin films can be due to a reduction in the active surface area of TiO_2 nanoparticles (those making direct contact with contaminated water) because the SOG-based oxide will cover some surface areas of TiO_2 avoiding its direct contact with water so that generation of hydroxyl radicals may be reduced. Also, low-temperature SOG-based oxide may create trap centers for some of the electron–hole pairs (being generated in TiO_2 after UV irradiation) so that the final effect is a reduced number of radicals that can efficiently inactivate bacteria present in water. Nonetheless, these results show moderate bacteria inactivation activity for thin films based on rutile TiO_2 nanoparticles (after very low thermal processing), and their activity could be enhanced if we increase the TiO_2 nanoparticle concentration, the film's surface area, or by including some anatase TiO_2 nanoparticles as well.

Conclusions

Rutile phase, undoped TiO_2 nanoparticles were processed at low temperatures and deposited as thin films on glass surfaces showing moderate efficiency for bacteria inactivation under UV–A radiation. We found that higher concentrations of TiO_2 nanoparticles (embedded within an inorganic matrix of SOG-based SiO_2) produce thicker films, while a more efficient yet moderate inactivation of *E. coli* is also obtained. The evidence of the rutile phase for the TiO_2 nanoparticles is provided by XRD measurements, while the presence of Ti–O bonds for TiO_2/SiO_2 deposited on glass confirms that inactivation of *E. coli* in water is directly related to specific concentration ratios of this photocatalytic material. From UV–Vis spectroscopy, the calculated band-gap energy for TiO_2/SiO_2 films was 3.11 eV and is independent of film thickness. From bacteria inactivation results, it is clear that rutile phase, undoped TiO_2 (in suspension form) presents similar yet slower activity characteristics when compared with anatase phase TiO_2. For thin films based on rutile TiO_2, the bacteria inactivation properties are reduced and only observed for the highest concentration ratios. For practical water decontamination, the suspension form of TiO_2 nanoparticles (rutile or anatase) is not desired because of the problem to remove this catalyst off the cleaned water. Therefore, it is important to find the best matrix to immobilize the TiO_2 nanoparticles and also, increase their concentration in the resulting films to obtain more efficient generation of hydroxyl radicals and have a system without suspended particles at the end of the process. Finally, by using low-temperature, simple, and economic processing techniques, immobilization of TiO_2 nanoparticles in a suitable inorganic matrix for bacteria inactivation was demonstrated and this process could be applied to more efficient water decontamination in places having strong UV irradiation.

Acknowledgements J. Molina thanks Alfredo Morales S. (Centro de Investigacion en Materiales Avanzados, CIMAV) for the latter's support on XRD measurements. This study was fully supported by the National Council of Science and Technology (CONACYT-Mexico).

References

1. Qu X, Alvarez PJJ, Li Q (2013) Water Res 47(12):3931
2. Chong MN, Jin B, Chow CWK, Saint C (2010) Water Res 44(10):2997
3. Dey T (ed) (2012) Nanotechnology for water purification. Brown Walker Press, Boca Raton
4. Banerjee AN (2011) Nanotechnol Sci Appl 4(1):35
5. Nakata K, Fujishima A (2012) J Photochem Photobiol C 13(3):169
6. Ding Z, Lu GQ, Greenfield PF (2000) J Phys Chem B 104(19):4815
7. Kandiel TA, Dillert R, Feldhoff A, Bahnemann DW (2010) J Phys Chem C 114(11):4909
8. Behnajady MA, Modirshahla N, Shokri M, Rad b (2008) Glob NEST J 10(1):1
9. Kim DH, Choi DK, Kim SJ, Lee KS (2008) Catal Commun 9(5):654
10. He J, Liu Q, Sun Z, Yan W, Zhang G, Qi Z, Xu P, Wu Z, Wei S (2010) J Phys Chem C 114(13):6035
11. Diwald O, Thompson TL, Goralski EG, Walck SD, Yates JT (2004) J Phys Chem B 108(1):52
12. Valentin CD, Pacchion G, Selloni A (2004) Phys Rev B 70(8):085116
13. Hsu SW, Yang TS, Chen TK, Wong MS (2007) Thin Solid Films 515(7–8):3521
14. Molina J, Munoz AL, Torres A, Landa M, Alarcon P, Escobar M (2011) Mater Sci Eng B 176(17):1353
15. Tauc J (1968) Mater Res Bull 3(1):37
16. Pankove JI (ed) (1984) Semiconductors and semimetals, part B optical properties, chap 2: the optical absorption edge of a-Si: H. Academic Press, New York, p 11
17. Music S, Vincekovic NF, Sekovanic L (2011) Braz J Chem Eng 28(1):89
18. Lopez T, Sanchez E, Bosch P, Meas Y, Gomez R (1992) Mater Chem Phys 32(2):141
19. Murashkevich AN, Lavistkaya AS, Barannikova TI, Zharskii IM (2008) J Appl Spectrosc 75(5):730
20. Goldstein DN, McCormick JA, George SM (2008) J Phys Chem C 112(49):19530

21. Maira AJ, Coronado JM, Augugliaro V, Yeung KL, Conesa JC, Soria J (2001) J Catal 202(2):413
22. Swanepoel R (1983) J Phys E 16(1):1214
23. Sreemany M, Sen S (2004) Mater Chem Phys 83(1):169
24. Dharma J, Pisal A (2012) Simple method of measurement the band gap energy value of TiO_2 in the powder form using UV/Vis/NIR spectrometer. Application Note. PerkinElmer Inc., Shelton
25. Valencia S, Marin JM, Restrepo G (2010) Open Mater Sci J 4(1):9